Improved Belief Propagation Decoding algorithms for surface codes

Jiahan Chen,¹ Zhengzhong Yi,^{1,*} Zhipeng Liang,¹ and Xuan Wang^{1,†}

¹ Harbin Institute of Technology, Shenzhen, China

(Dated: July 16, 2024)

Quantum error correction is crucial for universal fault-tolerant quantum computing. Highly accurate and low-time-complexity decoding algorithms play an indispensable role in making sure quantum error correction works. Among existing decoding algorithms, belief propagation (BP) is notable for its nearly linear time complexity and general applicability to stabilizer codes. However, BP's decoding accuracy without post-processing is unsatisfactory in most situations. This article focuses on improving the decoding accuracy of BP over GF(4) for surface codes. We first propose Momentum-BP and AdaGrad-BP, inspired by machine learning optimization techniques, to reduce oscillation in message updating and break the symmetric trapping sets. We further propose EWAInit-BP, which adaptively updates initial probabilities and provides a 1 to 3 orders of magnitude improvement over traditional BP for planar surface code, toric code, and XZZX surface code without any post-processing method, showing high decoding accuracy even under parallel scheduling. The theoretical O(1) time complexity under parallel scheduling and high accuracy of EWAInit-BP make it a promising candidate for high-precision real-time decoders. Meanwhile, the ideas of the Momentum-BP, AdaGrad-BP and EWAInit-BP provide promising approaches to improve the decoding accuracy of BP to get rid of its reliance on post-processing.

I. INTRODUCTION

Information in quantum computing devices is highly susceptible to noises, leading to information loss and computational errors [1]. To address this issue, quantum error correction (QEC) introduces redundant physical qubits and encodes the information in certain subspace of the state space of all the physical qubits to protect the information. So far at least, QEC is an essential step towards universal fault-tolerant quantum computation [2–4]. To make sure QEC work, the decoder of a QEC code should output the estimation of error fast and accurate according to the error syndromes.

Several decoding algorithms have achieved notable success, including the minimum-weight perfect matching (MWPM) [5] algorithm, union-find (UF) algorithm [6], maximum likelihood (ML) algorithm [7], matrix-productstates-based (MPS-based) algorithm [7], renormalization group algorithm [8], and neural-network-based (NNbased) algorithm [9–16]. Among these, ML, MWPM, and MPS-based algorithms offer high accuracy but come with high complexity. In contrast, the UF algorithm provides near-linear complexity with slightly lower accuracy. NN-based decoders have to balance scalability, decoding accuracy, and time cost [13], and may struggle with generalizability across different codes. Consequently, existing decoding algorithms rarely meet the requirements for both high accuracy and low complexity in quantum error correction decoding [17, 18].

Belief Propagation (BP) algorithm [19] are applicable to any stabilizer code and can achieve a complexity of $O(j\tau N)$ [20], where j is the average weight of the

rows/columns of the check matrix, and τ is the number of iterations. Additionally, parallel scheduling of BP can be efficiently implemented in hardware, theoretically achieving constant-time complexity [21]. However, traditional BP exhibit low decoding accuracy for many quantum error correcting codes and even cannot achieve the code capacity threshold for surface codes.

BP can be implemented over both GF(4) [20, 22–27] and GF(2) [28–31], where the Pauli operators are represented. There have been some efforts improving decoding accuracy of BP over GF(4) and GF(2). Over GF(4), MBP [20] achieves a threshold of 14.5% to 16% of the planar surface code by modifying the step size in the a posteriori probability updating. However, MBP is limited to serial scheduling, and the outer loop for searching step sizes increases its time complexity. Over GF(2), GBP [31] achieves a 14% threshold by combining generalized belief propagation with multiple rounds of decoding. This algorithm can be implemented in parallel, but the number of outer loops increases with the code length, adding to its time complexity. BP-OTS [32] periodically detects and breaks trapping sets using manually set parameters, allowing parallel implementation while maintaining the original complexity. It outperforms MBP for short codes but does not achieve a significant threshold.

Post-processing methods, such as OSD, SI (stabilizer inactivation) [33], MWPM [34–36] and UN[3] are often used to improve BP's decoding accuracy. However, they also introduce extra time cost and all have high time complexities, ranging from $O(N^2)$ to $O(N^3)$. Improving BP's decoding accuracy to get rid of its reliance on post-processing algorithms remains a significant challenge.

In this article, we mainly focus on improving BP's decoding accuracy for surface codes. However, we believe that the idea used in these improvements will also work for some other stabilizer codes. There are several explanations for why surface codes are challenging for BP

^{*} zhengzhongyi@cs.hitsz.edu.cn

[†] wangxuan@insun.hit.edu.cn

decoding. From the perspective of degeneracy [20, 37], stabilizers of surface codes have much lower weights compared to the code distance, leading to multiple low-weight errors corresponding to the same syndrome, thus having negative influence on BP's error convergence. From the perspective of short cycles [19], a number of 4-cycles over GF(4) and 8-cycles over GF(2) in surface codes can cause BP's inaccurate updating. A more intuitive explanation involves trapping sets [32, 38], where surface codes have many symmetric trapping sets causing BP messages to oscillate periodically.

This article employs three strategies to improve BP: optimizing message updates by optimization methods in machine learning, and optimizing a priori probabilities by utilizing a posteriori probabilities output by previous iterations. First, inspired by the similarity between BP message update and gradient descent of the energy function, we leverage optimization methods in machine learning to optimize the message update rules, and proposed Momentum-BP and AdaGrad-BP. In addition to improving decoding accuracy, experiments on trapping sets in surface codes show that Momentum-BP and AdaGrad-BP can smooth the message update process and reduce oscillation amplitude.

Furthermore, realizing the importance of a priori and a posteriori probabilities involved in the iteration of BP, we propose EWAInit-BP which dynamically updates the a priori probabilities involved in each iteration by utilizing the a posteriori probabilities output by previous iterations. Experiments on short toric codes, planar surface codes, and XZZX surface codes (under bias noise) show that, under both parallel scheduling and serial scheduling, EWAInit-BP outperforms existing BP improvements without post-processing and outer loops. Notably, the time complexity of all proposed improvements remains $O(j\tau N)$. Thus, EWAInit-BP can be implemented with theoretical constant complexity in parallel while maintaining decoding accuracy.

The structure of this article is as follows. Section II introduces the fundamentals of surface codes and BP decoding, as well as the perspective of BP as a gradient optimization, and summarizes the challenges BP faces in decoding surface codes. Section III introduces Momentum-BP, AdaGrad-BP and EWAInit-BP. The results of the simulation are presented in Section IV. Section V summarizes our work and discusses the future challenges.

II. PRELIMINARIES

A. Surface codes

A stabilizer code is defined by an abelian subgroup S of the Pauli group \mathcal{P}_n excluding -I, composed of operators $S \in \mathcal{P}_n$ such that $S|\psi\rangle = |\psi\rangle$ for all codewords $|\psi\rangle$ in the code space. The code space is the simultaneous +1 eigenspace of all elements of S. The stabilizers

must commute with each other, which means $[S_i, S_j] = 0$ for $\forall S_i, S_j \in \mathcal{S}$. The dimension of the code space is determined by the number of independent generators of \mathcal{S} . For a stabilizer code with N physical qubits and K logical qubits, \mathcal{S} has N - K independent generators.

The stabilizers are used to detect errors by measuring their eigenvalues. The set of measurement outcomes, known as the *error syndrome*, contains some information about the errors on physical qubits. The logical operators of a stabilizer code are Pauli operators that commute with all elements of \mathcal{S} but are not in \mathcal{S} , thus in $\mathcal{N}(\mathcal{S}) \setminus \mathcal{S}$ where $\mathcal{N}(\mathcal{S}) = \{E: ES = SE, \ \forall S \in \mathcal{S}\}$. They act on the encoded logical qubits without disturbing the code space. Due to this, the logical operators can be also regarded as *undetectable errors*, in the case that they are not performed on the physical qubits according to our requirements. The code distance D is defined as the minimum weight of logical operators. A quantum stabilizer code can be represented by [N, K, D].

The most eye-catching stabilizer codes in recent years might be surface codes. Surface codes are a class of quantum Low-Density Parity-Check (LDPC) codes [39] where qubits are placed on a 2-dimensional lattice, relying on the topology of the surface to protect quantum information [40]. Logical qubits are encoded in global degrees of freedom, and larger lattices provide larger code distances. There are some common properties of surface codes, such as the code distance scales with the code length as $O(\sqrt{N})$, while the code rate is asymptotically zero. In this article, toric codes refer to the ones with closed boundary, and planar surface codes refer to the ones with open boundary. The stabilizers of these two types are all Pauli X or Pauli Z. Besides, XZZX surface codes refer to the toric codes whose stabilizers are in the form of XZZX.

A $[[2L^2, 2, L]]$ toric code has a 2-dimensional torus topology, and the closed boundaries makes it translationally invariant to the error syndrome, which is beneficial to decoding algorithms (such as BP and neural networks). The Euler characteristic of the torus is 0, but the X-type and Z-type stabilizers of the toric code both have a redundancy, resulting in a total of two encoded logical qubits.

A $[[2L^2 - 2L + 1, 1, L]]$ planar surface code is defined on a surface with open boundaries, which makes the stabilizers near the boundaries having lower weights. This reduction in stabilizer weight results in a slight decrease in the error correction capability compared to the toric code, however, simplifies its implementation in physical quantum systems. The lattice structure of the planar surface codes are illustrated in Fig. 1.

A $[[L^2,2,L]]$ XZZX surface code is a non-CSS code designed to handle biased noise more effectively. The stabilizers of these codes have the form of XZZX. This alternating pattern of Pauli X and Z operators allows the code to reach the theoretical maximum threshold of 50% under pure Pauli X, pure Pauli Y and pure Pauli Z noise.

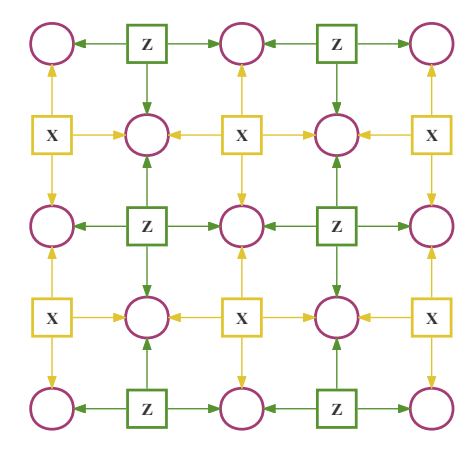


FIG. 1. The lattice of the $[[2L^2-2L+1,1,L]]$ planar surface code with L=3. Circles represent data qubits, yellow squares represent X-type stabilizers, green squares represent Z-type stabilizers, and arrows indicate the coupling between stabilizers and qubits.

B. Belief propagation decoding

1. $BP \ over \ GF(4)$

The idea of maximum likelihood decoding in quantum error correction is to find the most likely error coset given the error syndrome. This can be expressed as [22]

$$E = \arg\max_{ES} \sum_{S \in S} p(ES|s) \tag{1}$$

where the term ES denotes the coset formed by the error E and the stabilizer S. However, finding this maximum likelihood solution is computationally exponential [41]. Belief propagation decoding algorithm simplifies the above objective to

$$E = \left\{ \arg \max_{E_j} p(E_j|s) \right\}_{j=1}^n \tag{2}$$

where the probability of each individual error E_j given the syndrome s is maximized independently for j=1to n. Belief propagation makes two simplifications to the objective, compromising its performance on highly degenerate quantum codes.

- Assuming the most likely error pattern is the same as the most likely error coset;
- Assuming the most likely error on each qubit is the same as the most likely error pattern.

BP algorithm passes messages on a *Tanner graph*, where stabilizers and qubits are represented as *check nodes* and *variable nodes*, respectively. Over GF(4) which this article mainly focuses on, each variable node corresponds to a probability vector of all Pauli errors on one qubit.

Besides, one can use log-likelihood ratio (LLR) as the message passed between variable nodes and check nodes. In this way, belief propagation (abbreviated as LLR-BP₄) receives a priori probability vectors describing each type of Pauli error on each qubit $Q^{(0)} = \{p_{v_j}^X, p_{v_j}^Y, p_{v_j}^Z\}_{j=1}^N$, and initializes the variable-to-check messages as [20]

$$m_{v_j \to c_i}^{(0)} = \lambda_{H_{ij}}(Q_{v_j,e}^{(0)}) = \lambda_{H_{ij}} \left(\ln \frac{1 - p_{v_j}}{p_{v_i}} \right),$$
 (3)

where the lambda function is defined as

$$\lambda(p^X, p^Y, p^Z) = \ln \frac{1 + e^{-p^H_{ij}}}{e^{-p^X} + e^{-p^Y} + e^{-p^Z} - e^{-p^H_{ij}}}$$
(4)

indicating the log-likelihood ratio of whether the Pauli error E_i commutes with the stabilizer S_i .

One iteration of BP consists of one horizontal update, one vertical update and one hard decision. In the horizontal update, each check node calculates the feedback based on the messages received from the variable nodes but not from the target variable node in last vertical update, sending a check-to-variable message as follows

$$w = 2 \tanh^{-1} \left(\prod_{v_{j'} \in \mathcal{N}(c_i) \setminus v_j} \tanh \left(\frac{m_{v_{j'} \to c_i}^{(t-1)}}{2} \right) \right), \quad (5)$$

$$m_{c_i \to v_i}^{(t)} = (-1)^{s_i} * w.$$
 (6)

In the vertical update, variable nodes aggregate the messages from check nodes and, after a similar extrinsic calculation as above, send variable-to-check messages as follows

$$m_{v_j \to c_i}^{(t)} = \lambda_{H_{ij}} (Q_{v_j,e}^{(0)} + \sum_{\substack{c_{i'} \in \mathcal{M}(v_j) \setminus c_i \\ (e,H_{i;i}) = 1}} m_{c_{i'} \to v_j}^{(t)}).$$
 (7)

In the hard decision, variable nodes first accumulate the messages from all check nodes to calculate the *a posteriori* probability

$$Q_{v_j,e}^{(t)} = Q_{v_j,e}^{(0)} + \sum_{\substack{c_i \in \mathcal{M}(v_j) \\ \langle e, H_{ij} \rangle = 1}} m_{c_i \to v_j}^{(t)}.$$
(8)

Then, for each variable node, if all log-likelihood ratios for Pauli errors are greater than 0, then the hard decision result is I; otherwise, it is the Pauli error with the smallest LLR value. The hard decisions of all qubits combine to form the error estimate \hat{E} . If \hat{E} corrects the error syndrome, the algorithm converges; otherwise, it returns to the horizontal update for a new iteration. If the maximum number of iterations is reached, decoding is considered to have failed.

BP can be performed under either parallel or serial scheduling [42]. Under parallel scheduling, all variable

nodes and check nodes update their messages simultaneously at each iteration, allowing for hardware parallelization and constant time complexity. On the other hand, the serial scheduling updates the messages of variable nodes and check nodes sequentially. This method leads to faster convergence and slightly higher accuracy, though it has a more complex hardware implementation and higher time complexity.

2. BP as gradient optimization

Each iteration of BP can be interpreted as one step of gradient descent with a simplified step size on the following energy function [20, 43]

$$J_S(\Gamma) = -\sum_{i=1}^m 2 \tanh^{-1} \left((-1)^{s_i} \prod_{v_j \in \mathcal{N}(c_i)} \tanh\left(\frac{\lambda_{H_{ij}}(Q_{v_j})}{2}\right) \right). \tag{9}$$

The term inside the parentheses of the energy function J_S measures the discrepancy between the result of the current iteration and the actual error syndrome of stabilizer S_i . The smaller the energy function, the closer the BP iteration result is to the correct solution.

The target variables for gradient updates are the *a posteriori* estimates of the probability of each type of Pauli error occurring at each variable node. Specifically, for the $e \in \{X,Y,Z\}$ type Pauli error on the *n*-th variable node, the *a posteriori* probability update is

$$Q_{v_j,e}^{(t)} = Q_{v_j,e}^{(t-1)} - \alpha \frac{\partial J}{\partial Q_{v_j,e}^{(t-1)}},$$
(10)

where the partial derivative is

$$\frac{\partial J}{\partial Q_{v_j}^e} = -\sum_{\substack{c_i \in \mathcal{M}(v_j) \\ \langle e, H_{ij} \rangle = 1}} \widetilde{m}_{c_i \to v_j} \\
* \frac{\eta g_{ij}(\Gamma) e^{-Q_{v_j}^e}}{e^{-Q_{v_j}^Y} + e^{-Q_{v_j}^Z} - e^{-Q_{v_j}^{H_{ij}}}}, \quad (11)$$

where $\widetilde{m}_{c_i \to v_j}$ is the *a posteriori* probability summation term approximated using tanh

$$\widetilde{m}_{c_i \to v_j} = (-1)^{s_i} \prod_{v_{j'} \in \mathcal{N}(c_i) \setminus v_j} \tanh\left(\frac{\lambda_{H_{ij'}}(\Gamma_{v_{j'}})}{2}\right). \quad (12)$$

From this gradient optimization perspective, MBP [20] adjusts the "learning rate" of message updates to converge more quickly to the equivalent energy minimum, which is common in degenerate quantum codes.

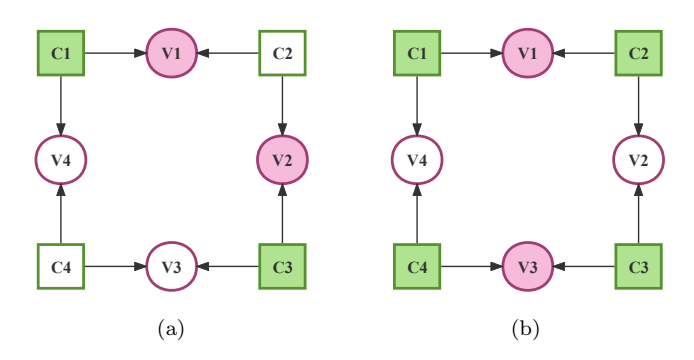


FIG. 2. Trapping sets with two types of error patterns in surface codes. Solid circles represent error qubits, and solid squares represent stabilizers with non-trivial error syndromes. The stabilizers in the figure can be either all X-type or all Z-type.

3. Hardness of BP in decoding surface codes

The decoding accuracy of BP in decoding surface codes is unsatisfactory due to several reasons, including cycles, degeneracy and trapping sets.

- a. Cycles Short cycles cause the joint probability calculations in BP to be dependent, which violates the independence assumption of updating variable nodes Eq. (7) and check nodes Eq. (5) [19]. Surface codes exhibit 8-cycles over GF(2) and 4-cycles over GF(4), exacerbating this issue.
- b. Degeneracy High degeneracy leads to BP decoding objectives Eq. (2) deviating from true targets Eq. (1) [22, 37]. This problem becomes particularly severe when errors can combine with stabilizers to form error types that are symmetric to original ones. In such cases, BP's marginal probability calculations for the both error types will be completely consistent. In surface codes, weights of the stabilizers are all no greater than 4, often much less than the weights of the logical operators. This symmetric degeneracy results in incorrect convergence of BP decoding.
- c. Trapping Sets Trapping sets are specific local structures in error-correcting codes combined with corresponding error patterns, where iterative decoding algorithms can never converge [44–46]. In quantum error correction, trapping sets are caused by the aforementioned short loops and symmetric degeneracy [38, 47]. The smallest trapping set in surface codes is shown in Fig. 2, consisting of an 8-cycle and four symmetric stabilizers, where the local connections of each check node and variable node are identical [32]. If any two qubits in this trapping set experience errors that anticommute with the stabilizers, the hard decision result of BP will oscillate periodically between all 0s and all 1s.

Optimizing BP from the first two perspectives involves modifying the underlying principles of the algorithm. This article will focus on trapping sets and seek methods to break the symmetry in message passing.

III. BELIEF PROPAGATION OPTIMIZATION

Surface codes violate the assumptions of BP's objective function and probability independence, making BP decoding difficult to converge. These issues are manifested in symmetric trapping sets, where the local structure of each node is identical, and message updates are symmetric under specific error patterns. Breaking the former symmetry involves modifying the code structure, while in this section, we focus on breaking the latter, the symmetry of message updates.

Message update optimization

1. Update smoothing

The Exponential Weighted Average (EWA) updates and smooths data series by combining the current observation with a weighted average of the previous value, expressed as

$$v_t = \gamma v_{t-1} + (1 - \gamma) x_t, \tag{13}$$

where x_t is the observation at time t, v_t is the smoothed value, and γ is a decay factor.

In the field of machine learning, momentum methods utilize an idea similar to EWA, adding a momentum term to allow gradient descent to accumulate historical information

$$m_t = \gamma m_{t-1} + (1 - \gamma) \nabla J(\theta), \tag{14}$$

$$\theta = \theta - \alpha m_t, \tag{15}$$

where γ is the decay factor, m_t is the accumulated momentum term, $\nabla J(\theta)$ is the gradient of the loss function with respect to parameter θ , and α is the learning rate. This method integrates previous directions while updating each parameter, thereby smoothing the update direction.

BP decoding can be analyzed from the perspective of the energy function. The high degeneracy of surface codes causes the energy function to have many equivalent global minima within a neighborhood. In the case of symmetric trapping sets, BP's specific update step size causes the hard decision results to oscillate between adjacent erroneous solutions. We incorporate the concept of momentum into BP's a posteriori probability updates to solve this issue by breaking the symmetry in BP's message updates.

Momentum-BP can be implemented under both parallel and serial scheduling. Here, we provide the latter in algorithm 1, where the initialization and check node update remain the same as in traditional BP. Our approach computes the a posteriori probability before performs the vertical update. The posterior update rule of Momentum-BP is shown as Eq. (16) and Eq. (17) where $g_{v_j,e}^{(t)}$ are the accumulated momentum term and $Q_{v_j,e}^{(t)}$ are the *a posteriori* probability for the *j*-th variable node regarding the Pauli error e in the t-th iteration. Notice that we transformed Eq. (8), so that the accumulated term is the posterior value from the previous iteration. In the variable node update step, we subtract the original message sent from the check node rather than the momentum-smoothed message to ensure stability and prevent overcompensation.

Algorithm 1 Momentum-BP under Serial Scheduling over GF(4)

Input: Parity-check matrix \mathbf{H} of $M \times N$, syndrome vector $s = (1, -1)^M$, a priori probability vectors $\{p_{v_j}^X, p_{v_j}^Y, p_{v_j}^Z\}_{j=1}^N$, max iterations $iter_{max}$, learning rate $\alpha = 1$, and momentum rate $\gamma > 0$.

Output: Estimated error vector \hat{E} .

Initialization:

for
$$j=1 \rightarrow N, \ e \in \{X,Y,Z\}$$
, do Initialize $Q_{v_j,e}^{(0)}$ as Eq. (3) Serial update:

for
$$j = 1 \to N, e \in \{X, Y, Z\}, do$$

for $i \in \mathcal{N}(v_j)$, do

Calculate $m_{c_i \to v_j}^{(t)}$ as Eq. (5)

Momentum update

$$g_{v_j,e}^{(t)} = \gamma g_{v_j,e}^{(t-1)} + (1 - \gamma) \frac{\partial J}{\partial Q_{v_j,e}^{(t-1)}}$$
(16)

$$Q_{v_j,e}^{(t)} = Q_{v_j,e}^{(t-1)} - \alpha g_{v_j,e}^{(t)}$$
(17)

Variable node update

$$m_{v_j \to c_i}^{(t)} = Q_{v_j,e}^{(t)} - \langle e, H_{ij} \rangle m_{c_i \to v_j}^{(t)}$$
 (18)

Hard decision:

$$\begin{aligned} &\text{for } j=1 \rightarrow N, \, e \in \{X,Y,Z\}, \, \mathbf{do} \\ &\text{if } Q_{v_j,e}^{(t)} > 0 \text{ for all } e, \, \mathbf{let } \, \hat{E}_i = I \\ &\text{else, let } \hat{E}_i = \mathop{\arg\min}_{e \in \{X,Y,Z\}} Q_{v_j,e}^{(t)} \end{aligned}$$

if $\langle H, \hat{E} \rangle = s$, return "converge" and halt. else if $t = iter_{max}$, return "fail" and halt. else repeat from serial update.

For the gradient calculation, we ignore the coefficient terms in Eq. (11), using the difference between the posterior updates calculated by traditional BP and the aposteriori probabilities from the previous iteration as the gradient for the current iteration, expanded in Eq. (19). When $\alpha = 1$ and $\gamma = 0$, Eq. (19) is equivalent to the traditional BP's a posteriori update; when $0 < \alpha < 1$ and $\gamma = 0$, it is equivalent to the EWA of a posteriori updates so far. In practice, to avoid the malice of hyperparameter tuning and to enhance the interpretability of the formula, we can either fix α at 1 or γ at 0.

$$Q_{v_j,e}^{(t)} = Q_{v_j,e}^{(t-1)} - \alpha \left(\gamma g_{v_j,e}^{(t-1)} + (1-\gamma)(Q_{v_j,e}^{(t-1)} - Q_{v_j,e}^{(0)} - \sum_{\substack{c_i \in \mathcal{M}(v_j)\\(e,H_{ij}) = 1}} m_{c_i \to v_j}^{(t)} \right)$$
(19)

$$\frac{\text{if }\alpha=1}{\prod_{v_{j},e}} \gamma (Q_{v_{j},e}^{(t-1)} - g_{v_{j},e}^{(t-1)}) + (1-\gamma)(Q_{v_{j},e}^{(0)} + \sum_{\substack{c_{i} \in \mathcal{M}(v_{j})\\(e,H_{ij})=1}} m_{c_{i}\to v_{j}}^{(t)}). \tag{20}$$

The properties of Momentum-BP can be explained from two perspectives. (1) Since it takes into account message updates from previous iterations, the method smooths the update direction in each iteration, preventing the corresponding energy function from oscillating between two points and gradually converging to the global minimum between them. (2) Node-wise momentum updates gradually break the symmetry of messages in the trapping sets shown in Fig. 2, allowing BP to escape from these trapping sets. The trapping set simulation in Section IV A will support those explanations.

2. Adaptive step size

The oscillation of message updates in trapping sets can also be attributed to the step size. In traditional LLR-BP, all variable node posterior updates result from directly accumulating messages from neighboring check nodes, which can become symmetric and cause oscillations. From the gradient perspective, if the step size is too large, the optimization algorithm is likely to oscillate; if the step size is too small, the algorithm is unable to update effectively. In practical decoding, the update frequency of different variable nodes may be uneven, with some requiring more rapid updates while others need to remain stable.

Inspired by adaptive gradient methods in deep learning, we propose AdaGrad-BP. The framework of this algorithm is very similar to Momentum-BP, with initialization and horizontal updates identical to traditional BP, while the posterior probability updates follow an adaptive step size rule, expressed as

$$Q_{v_j,e}^{(t)} = Q_{v_j,e}^{(t-1)} - \alpha \frac{g_{v_j,e}^{(t)}}{\sqrt{G_{v_j,e}^{(t)} + \epsilon}},$$
 (21)

where $g_{v_j,e}^{(t)}$ approximates the gradient of the energy function

$$g_{v_j,e}^{(t)} = Q_{j,e}^{(t-1)} - Q_{j,e}^{(0)} - \sum_{\substack{c_i \in \mathcal{M}(v_j) \\ \langle e, H_{ij} \rangle = 1}} m_{c_i \to v_j}^{(t)}, \qquad (22)$$

and $G_{v_j,e}^{(t)}$ is the cumulative sum of the squared gradients

as

$$G_{v_i,e}^{(t)} = G_{v_i,e}^{(t-1)} + (g_{v_i,e}^{(t)})^2.$$
(23)

This method adaptively alters the step size by accumulating historical gradient information. For instance, when the estimate of a variable node for a certain Pauli error changes significantly, the algorithm reduces the step size to counteract oscillation. Eq. (21) takes effect after the first iteration to ensure initial update stability. Here, α is the boost learning rate, providing an update impetus as the algorithm begins to accumulate gradients. This learning rate is relatively insensitive; a moderate value suffices. In all our tests, η is fixed at 5. While AdaGrad-BP may face issues with accumulated gradients causing the step size to approach zero after many iterations, this does not significantly impact the algorithm. In practice, AdaGrad can reduce the number of iterations, allowing most error patterns to converge before the gradients become too small.

Regrettably, combining Momentum-BP and AdaGrad-BP using the Adam optimizer or other methods has not yielded satisfactory results. On one hand, the Adam algorithm introduces additional hyperparameters whose optimal values for BP decoding cannot be directly borrowed from deep learning, thereby complicating the algorithm. On the other hand, Momentum and AdaGrad approach similar message update optimizations from different perspectives, and a straightforward combination of the two can lead to overcompensation.

B. EWA Initialization of a priori probability

BP decoding and gradient descent still have a fundamental difference, which limits the performance of algorithms in Section III A. Each update in gradient descent is based on the previous step's results, whereas in BP decoding, each calculation of a posteriori probabilities accumulates the same a priori probabilities. Given the objective function as shown in Eq. (2), for simplicity using the binary domain for instance, BP calculates the

LLR values as

$$Q_{v_j} = \ln \frac{P(e_j = 0|s)}{P(e_j = 1|s)}$$
(24)

$$= \ln \frac{P(e_j = 0) \cdot P(s|e_j = 0)}{P(e_j = 1) \cdot P(s|e_j = 1)}$$
 (25)

$$= \ln \frac{P(e_j = 0) \cdot P(s|e_j = 0)}{P(e_j = 1) \cdot P(s|e_j = 1)}$$

$$= Q_{v_j}^{(0)} + \sum_{c_{i'} \in \mathcal{M}(v_j) \setminus c_i} m_{c_{i'} \to v_j},$$
(25)

where $Q_{v_j}^{(0)}$ is a manually set initial value of the algorithm that participates in each iteration's *a posteriori* probability update. However, since the prior error probabilities are derived from an theoretical channel which is hard to measure and estimate in experiments, the a priori probabilities can significantly affect the BP iterations.

Existing methods for altering initial probabilities include re-initialization using information obtained from previous iterations [22, 23, 31], as well as detecting oscillations during the decoding process and modifying initial values accordingly [32]. However, they either require multiple outer loops or manually set algorithm parameters. This subsection introduces a method for dynamically updating a priori probabilities, employing a transformed exponential weighted averaging, incorporating components of all previous a posteriori probabilities into the a priori probabilities with a decaying factor. Hence, we call this method the EWAInit-BP. EWAInit-BP under parallel scheduling is shown in algorithm 2.

Algorithm 2 EWAInit-BP under Parallel Scheduling over GF(4)

Input: Parity-check matrix H, syndrome vector s, a priori LLR vectors $Q^{(0)}$, max iterations $iter_{max}$, discount factor α . Output: Estimated error vector \hat{E} .

EWA Initialization:

for $j = 1 \rightarrow N, e \in \{X, Y, Z\}$, do

$$\Pi_{v_j,e}^{(t)} = \alpha Q_{v_j,e}^{(0)} + (1-\alpha)Q_{v_j,e}^{(t-1)}$$
(27)

Horizontal update:

for $i = 1 \to M$, calculate $m_{c_i \to v_i}^{(t)}$ as Eq. (5)

Vertical update:

for $j = 1 \to N$, calculate $m_{v_j \to c_i}^{(t)}$ as Eq. (7)

Hard decision:

 $\begin{array}{l} \mbox{for } j=1 \rightarrow N,\, e \in \{X,Y,Z\}, \, \mbox{do} \\ \mbox{Calculate } Q_{v_j,e}^{(t)} \mbox{ as Eq. (8)} \end{array}$

if $Q_{v_j,e}^{(t)} > 0$ for all e, let $\hat{E}_i = I$ else, let $\hat{E}_i = \underset{e \in \{X,Y,Z\}}{\operatorname{arg min}} Q_{v_j,e}^{(t)}$

if $\langle H, \hat{E} \rangle = s$, return "converge" and halt. else if $t = iter_{max}$, return "fail" and halt. else repeat from EWA Initialization.

In fact, combining Eq. (27) and Eq. (8), EWAInit-BP exhibits similar characteristics to Momentum-BP, namely the exponentially decaying components of previous iterations. The difference is that the former aggressively changes the "prior" probability of each variable node in each iteration. Eq. (27) still retains a portion of the input prior probabilities. In our experiments, we tried replacing this term with the prior probabilities from the previous iteration, but the algorithm's performance did not significantly change.

Complexity

Our proposed algorithms involve the same message passing between variable nodes and check nodes as traditional BP. The main difference lies in the additional update steps, which in Momentum-BP and AdaGrad-BP consist of recalculating the a posteriori probabilities, and in EWAInit-BP involves recalculating the a priori probabilities. These additional steps only involve simple arithmetic operations and can be executed locally at each node, without requiring extra iterations, loops, or global communication, thus not introducing any significant overhead. Therefore, the overall time complexity of the proposed algorithms remains $O(j\tau N)$, where j is the average degree of the Tanner graph, and τ is the number of iterations.

In terms of space complexity, traditional BP requires storing messages and probability values, resulting in O(N) space requirements. Our algorithms only add extra storage space to accumulate gradients or maintain exponential weighted averages which is proportional to the number of variable nodes and does not change the overall space complexity. Thus, our improved algorithms maintain the same efficiency in both time and space as traditional BP, ensuring scalability and feasibility for practical implementation.

IV. SIMULATION RESULTS

In all simulations, the criterion for successful decoding is that the error estimate satisfies $\hat{E} \in ES$, rather than $\hat{E} = E$ as in classical information. All cases not meeting the above condition are referred to as logical errors in this article. Herein, a detected error refers to $\hat{E}E$ being anti-commutative with any one stabilizer $S \in \mathcal{S}$; an undetected error implies $\hat{E}E$ commutes with all stabilizers, i.e., $EE \in N(S) \setminus S$, where the result of error correction is a logical operator. Each data point on the experimental curves represents the mean of at least 10⁴ simulations.

Our simulations employ a depolarizing channel, where each qubit has an equal probability p/3 of experiencing Pauli X, Y, or Z errors, and a probability of 1-p of no error occurring. Additionally, for ease of comparison, we adopt the simple noise model which does not consider measurement errors or error propagation in quantum circuits.

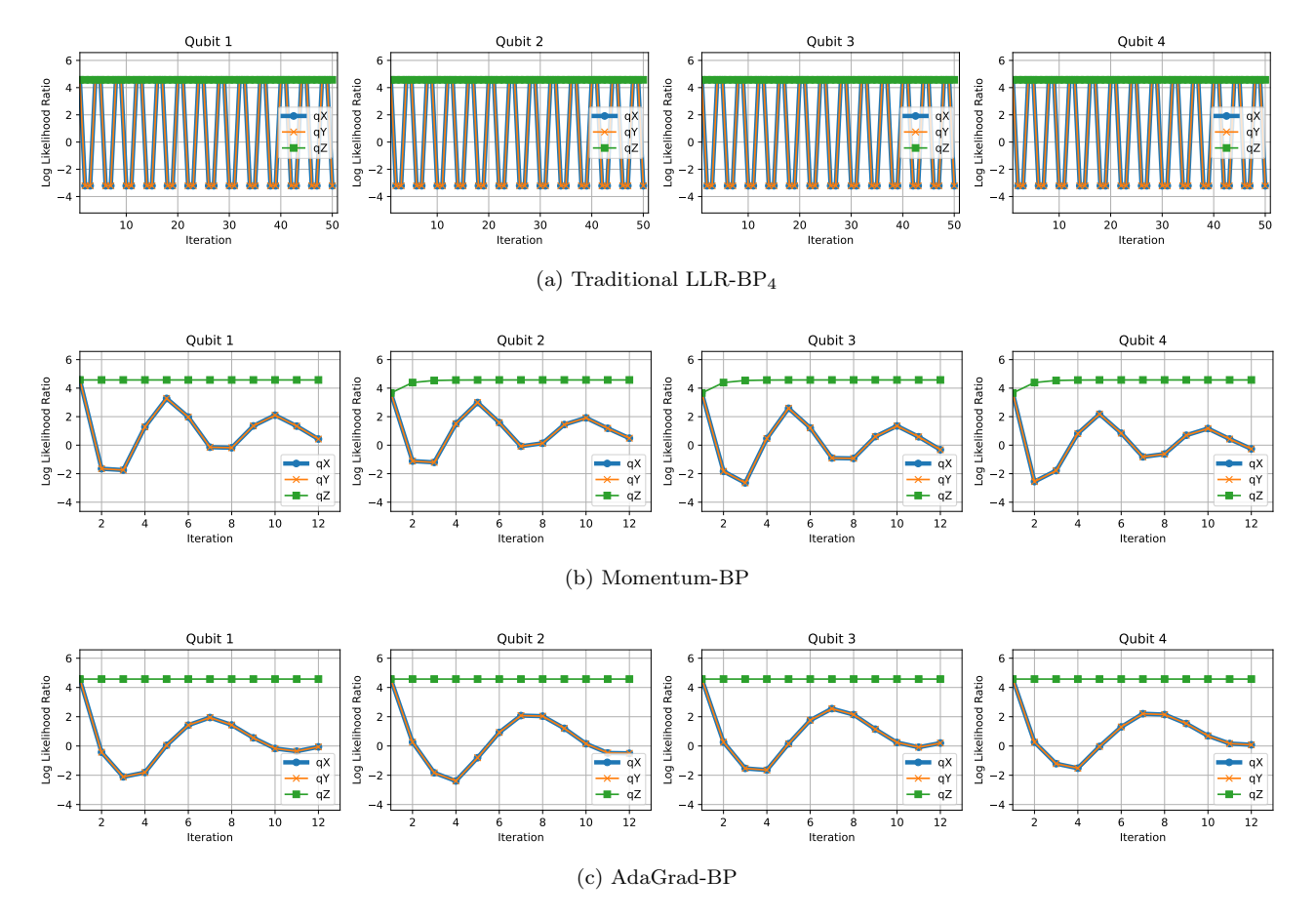


FIG. 3. Comparison of traditional LLR-BP₄, Momentum-BP, and AdaGrad-BP under parallel scheduling on the (4,0) trapping set. The latter two methods break the symmetry of message updates and converge within 12 iterations.

A. Breaking the Trapping Sets

We first compare the performance of improved BP on the trapping set shown in Fig. 2. In this example, qubit 1 and qubit 2 experience X errors, resulting in an error syndrome of [1,0,1,0]. Fig. 3 shows the comparison between the traditional LLR-BP₄, Momentum-BP and AdaGrad-BP in Section III A under parallel scheduling, with the maximum iteration set to 50. The hard decision result of the traditional BP oscillates continuously between all X and all I, while improved BP algorithms show significantly reduced oscillation amplitude and converge within 12 iterations.

A more detailed comparison of the different algorithms proposed in this article is presented in Table. I. The parameters used for these algorithms are defaults and were not specially optimized for this example. MBP [20] converges at the same fastest speed under serial scheduling but oscillates under parallel scheduling. BP-OTS [32] shows little dependency on scheduling method but its convergence depends on the manually set oscillation period T, which may vary in different error correction scenarios. Algorithms proposed in Section III A, Momentum-BP and AdaGrad-BP, both converge under

parallel scheduling. Besides, AdaGrad-BP and EWAInit-BP with adaptive *a priori* probabilities converge at the fastest speed under serial scheduling.

TABLE I. Iterations required by different BP algorithms on the (4,0) trapping set

Algorithm [48]	Parallel Scheduling	Serial Scheduling
LLR-BP ₄ [29]	_	
MBP [20]	_	2
BP-OTS [32]	T+2	T+2
EWAInit-BP		2
Momentum-BP	12	6
AdaGrad-BP	12	2

B. Improved BP on Topological codes

In this subsection, we compare the performance of various BP improvements proposed in this article. Subsequently, we present comparisons of our algorithm with other BP improvements without post-processing for toric codes, planar surface codes, and XZZX surface codes. For all decoding algorithms, the maximum number of it-

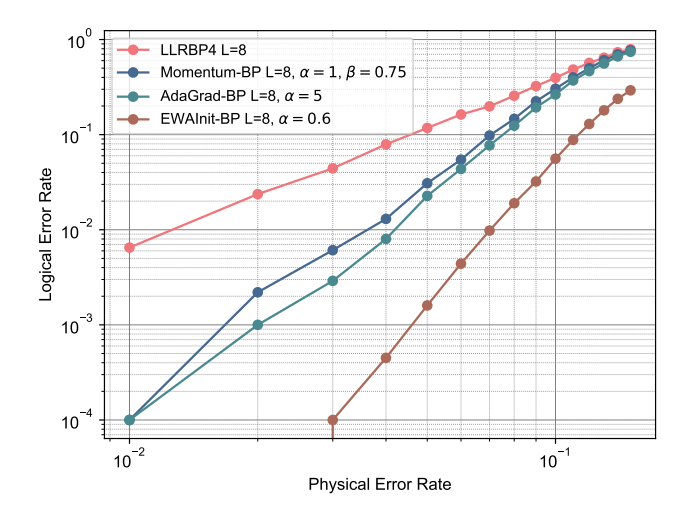


FIG. 4. Performance of various BP optimization methods presented in this article under serial scheduling, demonstrated using the L=8 toric code as an example. Each method uses default parameters. Among these, the method for optimizing initial values, EWAInit-BP, exhibits the best performance and completely eliminates the error floor.

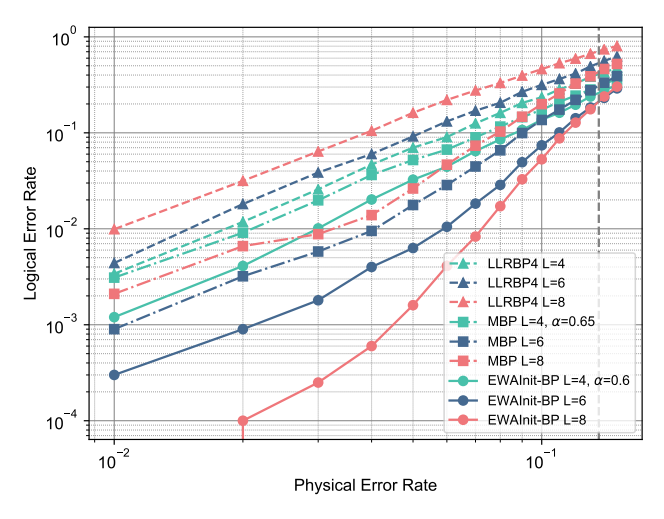
erations $iter_{max}$ across all code lengths is set to 150 to ensure linear asymptotic complexity.

1. Comparison of our BP optimization methods

A comparison of all methods proposed in this article is illustrated in Fig. 4. The two methods for optimizing message update rules, Momentum-BP and AdaGrad-BP, exhibit some improvements over traditional BP at low physical error rates, while their performance gradually converging to that of traditional BP as the physical error rate increases. The method for optimizing initial values, EWAInit-BP, demonstrate improvements ranging from 1 to 3 orders of magnitude over traditional BP, and excellently eliminate the error floor. However, the performance of algorithms that combine these two ideas is not satisfactory, because both approaches inherently consider the historical a posteriori probabilities but from different positions within the BP algorithm. This two methods are essentially addressing the same problem—incorporating past information to refine current updates. As a result, simply merging them can lead to redundancy and overcompensation, which negatively impacts the overall performance.

2. Toric code

We construct the $[[2n^2, 1, n]]$ toric code based on its properties as a hypergraph product of an [n, 1] repetition code. The toric code features periodic boundaries, hence all its stabilizers have a weight of four, and any er-



(a) Logical error rates

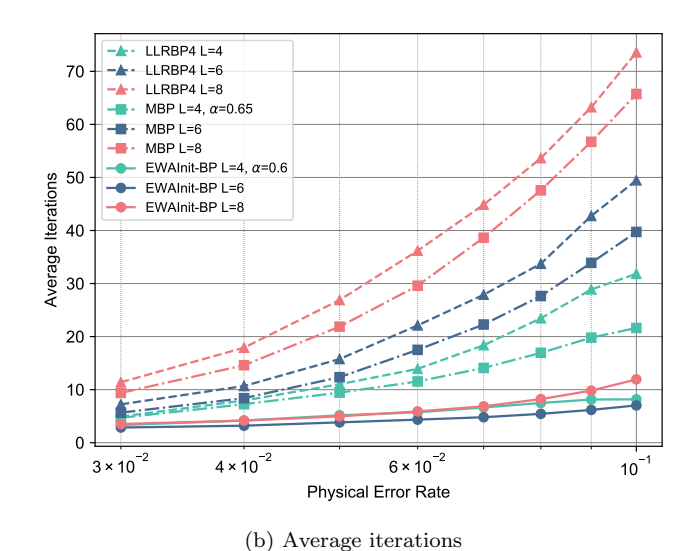
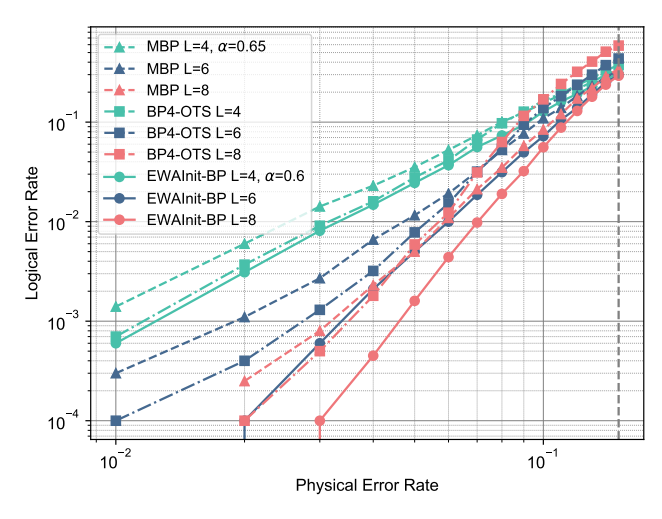


FIG. 5. Performance of LLRBP4, MBP, and EWAInit-BP under parallel scheduling for toric codes with $L=\{4,\,6,\,8\}$. Only EWAInit-BP find a reduction in the logical error rate as the lattice size increases, with the intersection of error rates occurring at 13.6%.

ror syndromes on it exhibit translational symmetry [16], which is particularly conducive to BP and neural network decoding. We compare the performance of our EWAInit-BP and other existing methods under both parallel and serial scheduling as shown in Fig. 5 and Fig. 6, respectively.

For the parallel schedule [49], compared to the classic BP over GF(4) with LLR message and its enhancement, MBP, our EWAInit-BP is the only method that achieves a decrease in logical error rates as the lattice size increases, with significant improvements in logical error rates at the same lattice size. The intersection of the error rate curves for these lattice sizes is approximately 13.6%. Additionally, the average number of iterations required for EWAInit-BP is significantly lower



(a) Logical error rates

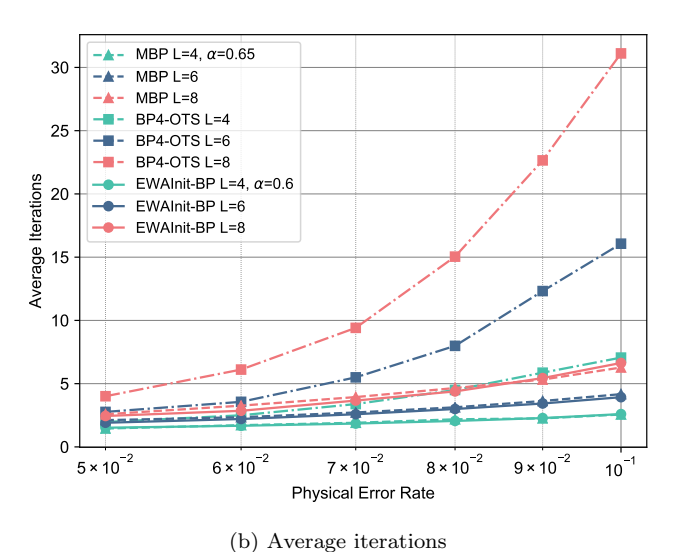


FIG. 6. Performance of MBP, BP-OTS, and EWAInit-BP under serial scheduling for toric codes with L = $\{4, 6, 8\}$. We choose T=9 and C=20 for BP-OTS. EWAInit-BP outperforms other BP improvements, with the intersection of logical error rates at 15%.

than the other two methods, converging in fewer than 10 iterations mostly. Parallel scheduling of BP algorithms holds the potential to achieve constant complexity through hardware-based parallel computation, while EWAInit-BP ensures both the error correction capabilities and speed in decoding.

For the serial schedule, all three decoding algorithms demonstrated error correction capabilities. Among those, BP-OTS performs better than MBP at low physical error rates, but its performance is surpassed by MBP when the physical error rate exceeds 7%. The performance of EWAInit-BP, on the other hand, consistently outperforms these two methods across all tested conditions, with the logical error rate at L=6 being comparable to that of the other two algorithms at L=8, and the in-

tersection of the logical error rate curves is approximately 15%. In terms of iteration count, both EWAInit-BP and MBP converge in remarkably few iterations (often fewer than 5).

It is noteworthy that for the toric code, the performance of EWAInit-BP under parallel scheduling is not significantly different from serial scheduling. This is due to the method's inherent ability to effectively break trapping sets, combined with the geometric symmetry of the Toric code, which allows for less dependency on the scheduling method. However, for the following topological codes with more complex stabilizer configurations, serial scheduling shows better performance.

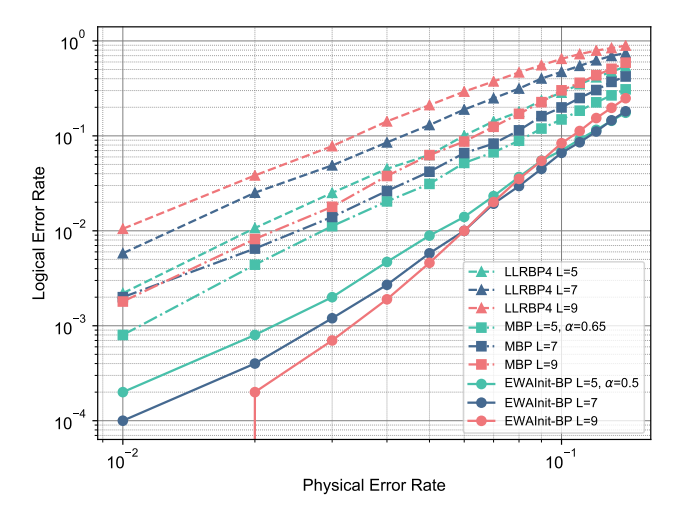
3. Planar surface code

The boundaries of the planar surface code are no longer contiguous, resulting in the emergence of some stabilizers with weight three and qubits that only connect two stabilizers at the boundaries. This configuration leads to a slight reduction in the error correction capabilities of the planar surface code compared to the Toric code. We compare the decoding logical error rates of LLRBP4, MBP, and EWAInit-BP under both parallel and serial scheduling, as illustrated in Fig. 7.

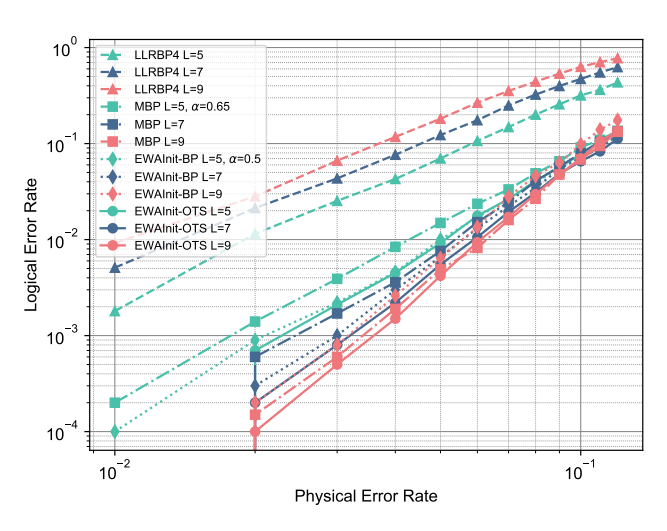
Under parallel scheduling, the decoding logical error rates of LLRBP4 and MBP4 increase with increasing code length, while EWAInit-BP achieves a reduction in logical error rates at low physical error rates. Unfortunately, at higher error rates, decoding at higher code lengths becomes more challenging, preventing EWAInit-BP from achieving a reliable threshold on the planar surface code.

Under serial scheduling, EWAInit-BP performs better than MBP at L=5 and L=7; however, its performance at L=9 is not satisfying. In fact, the decoding failure rate of EWAInit-BP increases with higher code lengths, thus not fully demonstrating the error-correcting capabilities of the code. This is because, despite the dynamic updating of a priori probabilities, the method still partly relies on the initial input priors. We incorporate the OTS method as a "post-processing" step for EWAInit, resetting the a priori probabilities of some nodes every few iterations, with the hyperparameters T=5 and C=20. This EWAInit-OTS method, while maintaining a time complexity of O(n), shows improvements in convergence rate and logical error rates on the surface code compared to EWAInit-BP and other methods.

The patterns of average iterations of different algorithms for the planar surface code and the XZZX surface code are similar to those observed in the toric code and exhibit the same trends as the logical error rates. Therefore, we have omitted this data.



(a) LER under a parallel schedule



(b) LER under a serial schedule

FIG. 7. Performance of LLRBP4, MBP, and EWAInit-BP (EWAInit-OTS) for planar surface codes with L = 5, 7, 9. The intersection of logical error rates for EWAInit-BP under serial scheduling is approximately 10%.

4. XZZX Surface code

For biased noise, the XZZX surface code exhibits superior error correction capabilities compared to the traditional planar surface code, achieving the theoretical maximum threshold of 50% across three types of pure Pauli error channels.

A comparison of decoding performance on the XZZX surface code is illustrated in Fig. 8. Our EWAInit combined with OTS method outperforms other algorithms under serial scheduling, with the LER curve intersection at approximately 12.4%. Unfortunately, for odd lattice sizes, the logical error rate for higher code lengths is higher than for lower code lengths at low physical error rates, while it demonstrates error-correcting capabilities

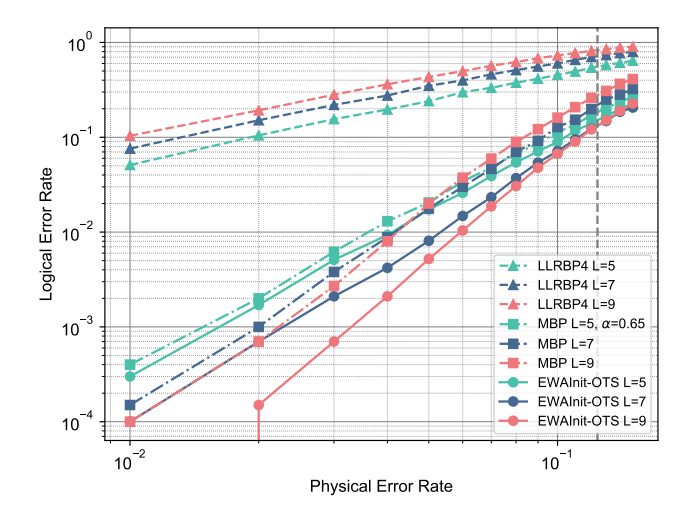


FIG. 8. Performance of LLRBP4, MBP, and EWAInit-BP (EWAInit-OTS) for XZZX surface codes with $L=5,\ 7,\ 9$ under serial scheduling. The intersection of logical error rates for EWAInit-BP is approximately 12.4%.

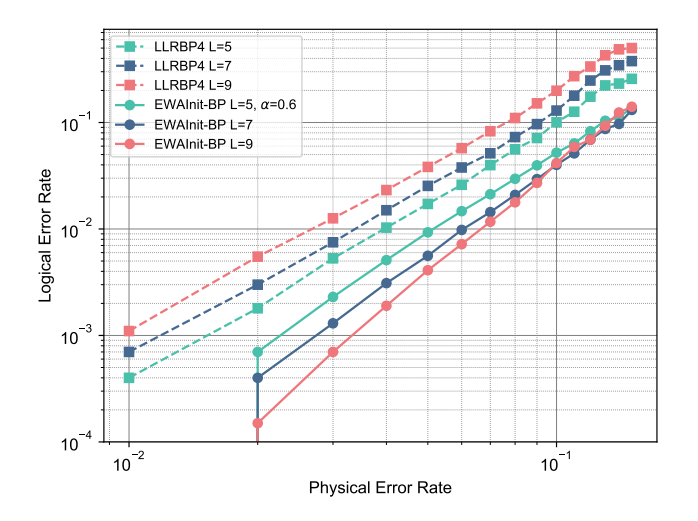


FIG. 9. Performance of LLRBP4 and EWAInit-BP for the XZZX surface code with $L=5,\,7,\,9$ under parallel scheduling, evaluated under conditions where Pauli Z errors are more prevalent in the channel. The intersection of LERs for EWAInit-BP is approximately 10%.

at higher physical error rates.

To demonstrate the bias noise correction capability of the XZZX surface code, we chose $p_z = \frac{2}{3}$ and $p_x = p_y = \frac{1}{6}$, implying that Pauli Z errors are more likely to occur, which aligns with the conditions found in actual hardware. Fig. 9 displays the decoding performance under biased noises under parallel scheduling. It is evident that when biased noise is present, the performance of BP decoding using the XZZX surface code with parallel scheduling shows significant improvement compared to that on a depolarizing channel. Besides, EWAInit-BP offers an improvement of approximately one order of

magnitude and demonstrates the error correction capability under parallel scheduling, with the intersection of logical error rates around 10%.

V. CONCLUSION

In this article, we proposed three improved BP algorithms which are Momentum-BP, AdaGrad-BP and EWAInit-BP.

Since the *a posteriori* probability update of BP can be interpreted as the gradient optimization of an energy function, we borrowed optimization strategies from gradient descent in machine learning, proposing Momentum-BP and AdaGrad-BP. These mechanisms aim to smooth the update process and reduce the amplitude of oscillations, respectively. Experiments on trapping sets intuitively demonstrated the effectiveness of these algorithms.

From the theoretical derivation of the message update rules of BP algorithm, we realized the importance of a priori probabilities and transformed the message update smoothing into initial values adapting, proposing EWAInit-BP. This algorithm exhibits aggressive exploration and outperforms other algorithms without OSD post-processing on the toric code, planar surface code, and XZZX surface code. Specifically, EWAInit-BP can demonstrate error correction capabilities even under parallel scheduling, with logical error rates decreasing as

code length increases. Notably, all our proposed methods do not introduce any additional factors to the time complexity of BP. Thus, EWAInit-BP can be implemented with O(1) complexity in fully parallel while maintaining decoding accuracy.

However, the aggressive exploration and convergence capabilities of EWAInit increase the probability of generating logical operators after error recovery. Therefore, directly applying this method to other error-correcting codes presents certain challenges. A potential research direction is to identify situations where logical operators may occur. Besides, our simulations only considered Pauli errors on qubits and did not account for measurement errors, error propagation in circuits, etc. Future work needs to adapt BP to more challenging noise models, potentially requiring specialized optimizations.

ACKNOWLEDGMENTS

We would like to express our sincere gratitude to Zhengzhong Yi for his in-depth discussions on the principles of BP algorithms and meticulous feedback on the manuscript. We are also thankful to Zhipeng Liang for his assistance with the experimental code framework. Finally, we extend our appreciation to Prof. Xuan Wang for his insightful discussions and guidance on the gradient approach.

- Y. Wang, M. Um, J. Zhang, S. An, M. Lyu, J.-N. Zhang, L.-M. Duan, D. Yum, and K. Kim, Single-qubit quantum memory exceeding ten-minute coherence time, Nature Photon. 11, 646 (2017).
- [2] Y. Zhao, Y. Ye, H.-L. Huang, Y. Zhang, D. Wu, H. Guan, Q. Zhu, Z. Wei, T. He, S. Cao, et al., Realization of an error-correcting surface code with superconducting qubits, Phys. Rev. Lett. 129, 030501 (2022).
- [3] G. Q. AI, Suppressing quantum errors by scaling a surface code logical qubit, Nature **614**, 676 (2023).
- [4] P. Shor, Fault-tolerant quantum computation, in Proceedings of 37th Conference on Foundations of Computer Science (1996) pp. 56–65.
- [5] J. Edmonds, Paths, trees, and flowers, Canad. J. Math. 17, 449 (1965).
- [6] N. Delfosse, V. Londe, and M. E. Beverland, Toward a union-find decoder for quantum ldpc codes, IEEE Trans. Inf. Theory 68, 3187 (2022).
- [7] S. Bravyi, M. Suchara, and A. Vargo, Efficient algorithms for maximum likelihood decoding in the surface code, Phys. Rev. A 90, 032326 (2014).
- [8] G. Duclos-Cianci and D. Poulin, Fast decoders for topological quantum codes, Phys. Rev. Lett. 104, 050504 (2010).
- [9] G. Torlai and R. G. Melko, Neural decoder for topological codes, Phys. Rev. Lett. 119, 030501 (2017).
- [10] N. P. Breuckmann and X. Ni, Scalable neural network decoders for higher dimensional quantum codes, Quantum

- **2**, 68 (2018).
- [11] Y.-H. Liu and D. Poulin, Neural belief-propagation decoders for quantum error-correcting codes, Phys. Rev. Lett. 122, 200501 (2019).
- [12] X. Ni, Neural network decoders for large-distance 2d toric codes, Quantum 4, 310 (2020).
- [13] K. Meinerz, C.-Y. Park, and S. Trebst, Scalable neural decoder for topological surface codes, Phys. Rev. Lett. 128, 080505 (2022).
- [14] R. W. J. Overwater, M. Babaie, and F. Sebastiano, Neural-network decoders for quantum error correction using surface codes: A space exploration of the hardware cost-performance tradeoffs, IEEE Trans. Quantum Eng. 3, 1 (2022).
- [15] Y. Choukroun and L. Wolf, Deep quantum error correction, in *Proceedings of the AAAI Conference on Artificial Intelligence*, Vol. 38 (2024) pp. 64–72.
- [16] P. Andreasson, J. Johansson, S. Liljestrand, and M. Granath, Quantum error correction for the toric code using deep reinforcement learning, Quantum 3, 183 (2019).
- [17] A. Holmes, M. R. Jokar, G. Pasandi, Y. Ding, M. Pedram, and F. T. Chong, Nisq+: Boosting quantum computing power by approximating quantum error correction, in 2020 ACM/IEEE 47th Annual International Symposium on Computer Architecture (ISCA) (2020) pp. 556–569.
- [18] F. Battistel, C. Chamberland, K. Johar, R. W. Overwa-

- ter, F. Sebastiano, L. Skoric, Y. Ueno, and M. Usman, Real-time decoding for fault-tolerant quantum computing: Progress, challenges and outlook, Nano Futures 7, 032003 (2023).
- [19] D. MacKay, G. Mitchison, and P. McFadden, Sparse-graph codes for quantum error correction, IEEE Trans. Inf. Theory 50, 2315 (2004).
- [20] K.-Y. Kuo and C.-Y. Lai, Exploiting degeneracy in belief propagation decoding of quantum codes, Npj Quantum Inf. 8, 111 (2022).
- [21] J. Valls, F. Garcia-Herrero, N. Raveendran, and B. Vasić, Syndrome-based min-sum vs osd-0 decoders: Fpga implementation and analysis for quantum ldpc codes, IEEE Access 9, 138734 (2021).
- [22] D. Poulin and Y. Chung, On the iterative decoding of sparse quantum codes (2008), arXiv:0801.1241.
- [23] Y.-J. Wang, B. C. Sanders, B.-M. Bai, and X.-M. Wang, Enhanced feedback iterative decoding of sparse quantum codes, IEEE Trans. Inf. Theory, 1231–1241 (2012).
- [24] Z. Babar, P. Botsinis, D. Alanis, S. X. Ng, and L. Hanzo, Fifteen years of quantum ldpc coding and improved decoding strategies, IEEE Access, 2492–2519 (2015).
- [25] N. Raveendran, M. Bahrami, and B. Vasic, Syndrome-generalized belief propagation decoding for quantum memories, in ICC 2019 2019 IEEE International Conference on Communications (ICC) (2019).
- [26] K.-Y. Kuo and C.-Y. Lai, Refined belief propagation decoding of sparse-graph quantum codes, IEEE J. Select. Areas Inform. Theory, 487–498 (2020).
- [27] K.-Y. Kuo and C.-Y. Lai, Comparison of 2d topological codes and their decoding performances, in 2022 IEEE International Symposium on Information Theory (ISIT) (2022) pp. 186–191.
- [28] A. Rigby, J. Olivier, and P. Jarvis, Modified belief propagation decoders for quantum low-density parity-check codes, Phys. Rev. A 100, 012330 (2019).
- [29] C.-Y. Lai and K.-Y. Kuo, Log-domain decoding of quantum ldpc codes over binary finite fields, IEEE Trans. Quantum Eng. 2, 1 (2021).
- [30] Z. Yi, Z. Liang, K. Zhong, Y. Wu, Z. Fang, and X. Wang, Improved belief propagation decoding algorithm based on decoupling representation of pauli operators for quantum ldpc codes (2023), arXiv:2305.17505.
- [31] J. Old and M. Rispler, Generalized belief propagation algorithms for decoding of surface codes, Quantum 7, 1037 (2023).
- [32] D. Chytas, M. Pacenti, N. Raveendran, M. F. Flanagan, and B. Vasić, Enhanced message-passing decoding of degenerate quantum codes utilizing trapping set dynamics, IEEE Commun. Lett. 28, 444 (2024).
- [33] J. D. Crest, M. Mhalla, and V. Savin, Stabilizer inactivation for message-passing decoding of quantum ldpc codes,

- in 2022 IEEE Information Theory Workshop (ITW) (2022) pp. 488–493.
- [34] B. Criger and I. Ashraf, Multi-path summation for decoding 2d topological codes, Quantum, 102 (2018).
- [35] O. Higgott, T. C. Bohdanowicz, A. Kubica, S. T. Flammia, and E. T. Campbell, Improved decoding of circuit noise and fragile boundaries of tailored surface codes, PRX Quantum 13, 031007 (2023).
- [36] L. Caune, B. Reid, J. Camps, and E. Campbell, Belief propagation as a partial decoder (2023), arXiv:2306.17142.
- [37] P. Fuentes, J. Etxezarreta Martinez, P. M. Crespo, and J. Garcia-Frías, Degeneracy and its impact on the decoding of sparse quantum codes, IEEE Access 9, 89093 (2021).
- [38] N. Raveendran and B. Vasić, Trapping sets of quantum ldpc codes, Quantum 5, 562 (2021).
- [39] N. P. Breuckmann and J. N. Eberhardt, Quantum lowdensity parity-check codes, PRX Quantum 2, 040101 (2021).
- [40] H. Bombin, An introduction to topological quantum codes (2013), arXiv:1311.0277.
- [41] M.-H. Hsieh and F. Le Gall, Np-hardness of decoding quantum error-correction codes, Phys. Rev. A 83, 052331 (2011).
- [42] D. Hocevar, A reduced complexity decoder architecture via layered decoding of ldpc codes, in *IEEE Workshop* on Signal Processing Systems, 2004. SIPS 2004. (2004).
- [43] R. Lucas, M. Bossert, and M. Breitbach, On iterative soft-decision decoding of linear binary block codes and product codes, IEEE J. Sel. Areas Commun., 276–296 (1998).
- [44] M. K. Dehkordi and A. H. Banihashemi, An efficient algorithm for finding dominant trapping sets of ldpc codes, in 2010 6th International Symposium on Turbo Codes; Iterative Information Processing (2010).
- [45] S. Han, J. Oh, K. Oh, and J. Ha, Deep-learning for breaking the trapping sets in low-density parity-check codes, IEEE Trans. Commun., 2909–2923 (2022).
- [46] S. Kang, J. Moon, J. Ha, and J. Shin, Breaking the trapping sets in ldpc codes: Check node removal and collaborative decoding, IEEE Trans. Commun. 64, 15 (2016).
- [47] A. K. Pradhan, N. Raveendran, N. Rengaswamy, X. Xiao, and B. Vasić, Learning to decode trapping sets in qldpc codes, in 2023 12th International Symposium on Topics in Coding (ISTC) (2023) pp. 1–5.
- [48] The parameters used for each algorithm are: MBP ($\alpha = 0.6$), Momentum-BP ($\alpha = 0.6$), AdaGrad-BP ($\alpha = 5$), EWAInit-BP ($\alpha = 0.6$).
- [49] Our implementation of BP-OTS over GF(4) under parallel scheduling did not achieve the performance reported in the original paper, necessitating further investigation into this discrepancy.